

Scene2BIR: Material-aware learning-based binaural impulse response generator for reconstructed real-world 3D scenes

ANTON JERAN RATNARAJAH, University of Maryland, USA
DINESH MANOCHA, University of Maryland, USA

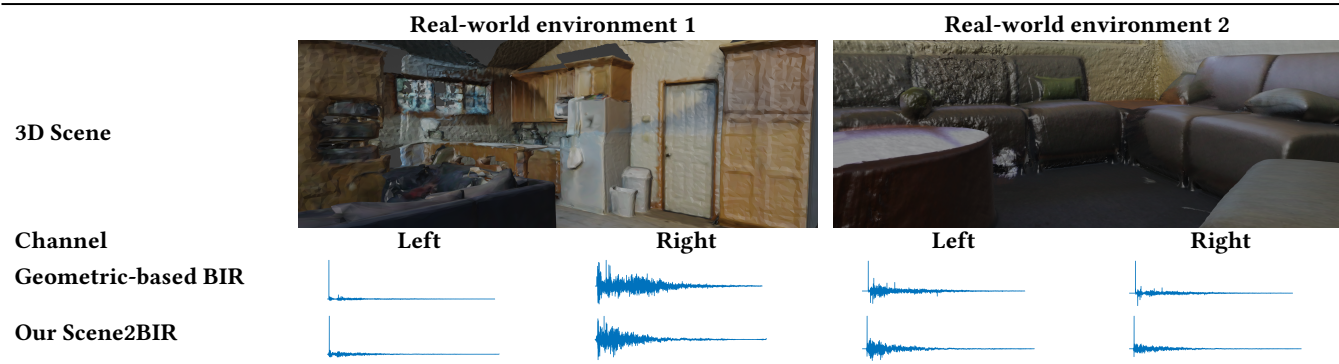


Fig. 1. The binaural impulse responses (BIRs) generated for real-world 3D reconstructed scenes. We compare the accuracy of our learning method (Scene2BIR) with geometric sound propagation algorithms. These models were not used in the training data for Scene2BIR. Our Scene2BIR can generate binaural IRs corresponding to left and high channels by taking into account interaural level differences (ILD) and interaural time differences (ITD). In practice, Scene2BIR is two orders of magnitude faster than the interactive geometric sound propagation algorithm. We will release the code and the dataset at the time of publication.

We present an end-to-end binaural impulse response generator (BIR) to generate plausible sounds in real-time for real-world models. Our approach uses a novel neural-network-based BIR generator (Scene2BIR) for the reconstructed 3D model. We propose a graph neural network that uses both the material and the topology information of the 3D scenes and generates a scene latent vector. Moreover, we use a conditional generative adversarial network (CGAN) to generate BIRs from the scene latent vector. Our network is able to handle holes or other artifacts in the reconstructed 3D mesh model. We present an efficient cost function to the generator network to incorporate spatial audio effects. Given the source and the listener position, our approach can generate a BIR in 0.1 milliseconds on an NVIDIA GeForce RTX 2080 Ti GPU and can easily handle multiple sources. We have evaluated the accuracy of our approach with real-world captured BIRs and an interactive geometric sound propagation algorithm.

We also performed a perceptual evaluation and observed that sounds generated by our approach are more plausible as compared to prior learning-based propagation algorithms.

CCS Concepts: • **Computing methodologies** → *Real-time simulation; Interactive simulation; Machine learning; Ray tracing.*

Authors' addresses: Anton Jeran Ratnarajah, University of Maryland, College Park, USA, jeran@umd.edu; Dinesh Manocha, University of Maryland, College Park, USA, dmanocha@umd.edu.

Permission to make digital or hard copies of all or part of this work for personal or classroom use is granted without fee provided that copies are not made or distributed for profit or commercial advantage and that copies bear this notice and the full citation on the first page. Copyrights for components of this work owned by others than ACM must be honored. Abstracting with credit is permitted. To copy otherwise, or republish, to post on servers or to redistribute to lists, requires prior specific permission and/or a fee. Request permissions from permissions@acm.org.

© 2023 Association for Computing Machinery.

0730-0301/2023/2-ART \$15.00

<https://doi.org/10.1145/nnnnnnnn.nnnnnnnn>

Additional Key Words and Phrases: sound propagation, learning-based, room materials

ACM Reference Format:

Anton Jeran Ratnarajah and Dinesh Manocha. 2023. Scene2BIR: Material-aware learning-based binaural impulse response generator for reconstructed real-world 3D scenes. *ACM Trans. Graph.* 1, 1 (February 2023), 12 pages. <https://doi.org/10.1145/nnnnnnnn.nnnnnnnn>

1 INTRODUCTION

Recent advances in computer vision and 3D reconstruction algorithms have made it possible to generate 3D models of real-world scenes [Dai et al. 2017a,b]. These reconstructed 3D models are used for visual analysis or interactive walkthroughs of buildings [Liu et al. 2015]. Furthermore, many tools or systems are available to transform real-life spaces into digital twin models, which offer higher visual fidelity than panoramic scans. The resulting models are used to generate immersive 3D experiences for VR (virtual reality) or AR (augmented reality) applications.

Many reconstructed models corresponding to apartments, houses, offices, public places, malls or tourist attractions consist of multiple sound sources (e.g., human speaker, dishwasher, telephone, music). In order to improve the sense of the presence of a user, it is important to augment the visual realism with sound effects generated by these sources. It is well known that a user's sense of presence in VR or AR environments can be improved by generating plausible sounds [Larsson et al. 2002]. The resulting sound effects vary based on the location of each source, the listener and the environment characteristics [Liu and Manocha 2022]. In practice, the sound effects in VR or AR environments can be modeled using impulse

responses (IRs), which capture how sound propagates from a source location to the position of the receiver in a given scene. IRs contain the necessary information for acoustic scene analysis such as the early reflections, late reverberation, arrival time, energy of direct and indirect sound, etc. The IR can be convolved with any dry sound (real or virtual) to generate the desired acoustic effects. Binaural IR (BIR) is the IR that characterizes the sound propagation from the sound source to the left and right ears of the listener. Unlike monaural IRs, binaural IRs have sufficient spatial information to locate the sound source accurately. Therefore BIRs give an immersive experience in AR and VR applications. It turns out that recording the BIRs in real-world scenes can be challenging and needs special capturing hardware. Furthermore, these BIRs need to be recaptured if the source or listener position changes.

In synthetic scenes, the IRs can be computed in real-time using sound propagation algorithms [Liu and Manocha 2022; Savioja 2010]. However, current propagation algorithms are limited to synthetic scenes where an exact geometric representation of the scene and acoustic material properties are known apriori. On the other, generating a large number of high-quality IRs for complex 3D real scenes in real-time remains a challenging problem [Chen et al. 2022].

Recently, neural-network-based IR generators have been proposed for interactive sound rendering applications [Luo et al. 2022; Ratnarajah et al. 2022b,c; Su et al. 2022]. After training, the network can be used to generate a large number of IRs for 3D scenes. However, current learning methods have some limitations. They only deal with the mesh geometry, compute monaural IRs, and do not consider the acoustic material properties of the objects in the 3D scene. The material acoustic properties depend on the surface roughness, thickness and acoustic impedance [Kuttruff 2016; Seddeq 2009]. The materials in the 3D scene strongly influence the overall accuracy of the IR by controlling the amount of sound absorption and scattering when the sound wave interacts with each surface in the scene. Moreover, current methods may not be directly applied to reconstructed 3D scenes with significant holes.

Main Results: We present a novel neural-network-based binaural impulse response (BIR) generator, Scene2BIR, to generate BIR for real 3D scenes in real-time. Our approach is general and can generate BIRs for arbitrary topologies and material properties in the 3D scenes, based on the source and the listener locations. Our network comprises a graph neural network to encode the 3D scene materials and the topology, and a conditional generative adversarial network (CGAN) conditioned on the encoded 3D scene to generate the BIRs. The CGAN consists of a generator and a discriminator network. Some of the novel components of our work include:

1. Material-aware learning-based method: We represent the material's acoustic properties using the frequency-dependent absorption and scattering coefficients. We calculate these material properties using average sound absorption and scattering coefficients for each vertex in a 3D scene from the input semantic labels of the 3D model and acoustic material databases. We propose an efficient approach to incorporate material properties in our Scene2BIR architecture. Our method results in more than 48% accuracy over prior learning methods in terms of acoustic characteristics of the IRs.

2. Binaural impulse response generation: We present a simple and efficient cost function to the generator network in our CGAN to incorporate spatial audio effects such as the difference in the time-of-arrival of sound arriving in left and right ears (interaural time difference) [Wightman and Kistler 1992] and sound level difference in both ears caused by the barrier created by the head when the sound is arriving (interaural level difference).

3. Perceptual evaluation: We performed a user study to evaluate the benefits of our material-aware BIR generator. The BIRs generated using our Scene2BIR change smoothly with the distance and the directions of the sound source. We observe increased perceptual differentiation in terms of plausibility over prior learning-based methods. More than 67% of the participants observe that the sound effects generated from Scene2BIR are more plausible than MESH2IR.

We generate 1 million high-quality BIRs using the geometric propagation method [Schissler and Manocha 2017] for around 1500 3D real-world scenes in the ScanNet dataset [Dai et al. 2017a]. Among 1 million BIRs, we randomly sampled 200,000 BIRs to train our network. We will release the full BIR dataset upon publication. We have evaluated the accuracy of our approach using the captured BIRs from the BRAS dataset [Aspöck et al. 2020] and synthetic BIRs generated using the geometric propagation approach for real scenes not used during training. Our network is capable of generating 10,000 BIRs per second for a given 3D scene on an NVIDIA GeForce RTX 2080 Ti GPU. In practice, we observe two orders of magnitude performance improvement over interactive sound propagation algorithms.

2 RELATED WORKS

Sound Propagation and IR Computation: The IRs can be computed using wave-based [Allen and Raghuvanshi 2015; Gumerov and Duraiswami 2008; Mehra et al. 2015; Thompson 2006] or geometric [Lentz et al. 2007; Schissler and Manocha 2011; Schissler et al. 2014] sound propagation algorithm. The wave-based algorithms are computationally expensive and their runtime is proportional to the third or fourth power of the highest simulation frequency [Raghuvanshi et al. 2009]. For interactive applications, IRs are precomputed for a 3D scene grid and at run time IRs are calculated for different listener positions using efficient interpolation techniques [Mehra et al. 2013; Raghuvanshi et al. 2010]. Geometric propagation algorithms are based on ray tracing or its variants and can be used for interactive applications [Chen et al. 2022; Schissler and Manocha 2017]. They can handle dynamic scenes and work well for high frequencies. Many hybrid combinations of geometric and wave-based methods have been proposed [Tang et al. 2021]. These methods are increasingly used for games and VR applications and can take tens of milliseconds to compute each IR on commodity hardware.

Learning-based IR generation: Learning-based IR computation algorithms have been proposed to generate IRs based on a single image of the environment [Kon and Koike 2019; Majumder et al. 2022; Singh et al. 2021], reverberant speech signal [Ratnarajah et al. 2022a; Steinmetz et al. 2021], or shoe-box shaped room geometry [Ratnarajah et al. 2022c]. Neural networks are also used to translate synthetic IRs to real IRs and to augment IRs [Ratnarajah et al. 2021a,b] and estimate room acoustic parameters [Eaton et al.

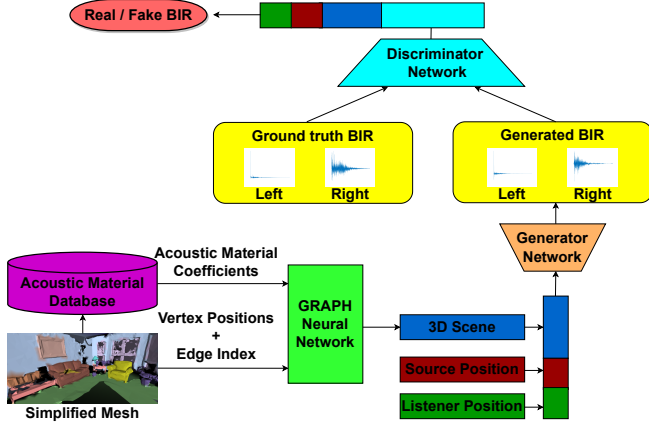


Fig. 2. The overall architecture of our Scene2BIR method: The simplified 3D scene mesh with material annotations is passed to the acoustic material database to estimate the acoustic material coefficients (absorption and scattering coefficient). We pass the acoustic material coefficients, vertex positions and edge index to our graph neural network (Fig. 4) to encode the 3D scene into a latent vector. Our generator network takes the 3D Scene and listener and source positions as input and generates a corresponding binaural impulse response (BIR). The discriminator network discriminates between the generated BIR and the ground truth BIR during training.

2016; Genovese et al. 2019; Savioja and Svensson 2015]. Learning-based approaches are proposed to learn the implicit representation of IRs for a given 3D scene and predict IRs for new locations on the same training scene [Luo et al. 2022; Su et al. 2022]. MESH2IR [Ratnarajah et al. 2022b] is an IR generator that takes the complete 3D mesh of a 3D scene and the source and the listener positions as input and generates monaural IRs in real-time on a high-end GPU. However, the sound rendered using these IRs generators may not be smooth and can have artifacts. Prior binaural IR generators require a few BIRs captured in a new 3D scene to generate new BIRs for different source and listener locations in the same 3D scene. Our learning-based method is more accurate and general than prior methods.

Real-world Scenes. The materials in the real-world scene influence the sound effects corresponding to the scene. The material information can be estimated from images and videos of real-world scenes and given as input to sound propagation algorithms using material acoustic coefficients [Brinkmann et al. 2019; Schissler et al. 2017; Tang et al. 2020]. Other methods are based on capturing reference audio samples or IRs in real-world scenes and the simulated IRs are adjusted to match the materials using reference audios or IRs [Li et al. 2018; Ren et al. 2013; Tang et al. 2020]. In recent works, real scenes are annotated using crowd-sourcing [Dai et al. 2017a] and material acoustic coefficients can be estimated by mapping the real scenes’ annotated material labels to materials in the existing acoustic coefficient database [Chen et al. 2022; Tang et al. 2022]. As compared to these methods, our approach is either significantly faster or generates higher-quality sound effects in real-world scenes.

3 MODEL REPRESENTATION AND DATASET GENERATION

Our approach is designed for real-world scenes. We use state-of-the-art methods in computer vision to reconstruct 3D scenes using RGB-D data captured using commodity devices (e.g., iPad and Microsoft Kinect). These reconstructed 3D scenes are segmented and the objects in the 3D scene can be annotated by crowdsourcing [Dai et al. 2017a,b]. Our goal is to use these mesh representations and semantic information to generate plausible sound effects. An overview of our approach is given in Fig. 2.

We preprocess the annotated 3D scene to close the holes in the reconstructed 3D scene and simplify the 3D scene by reducing the number of faces. We perform mesh simplification using graph processing to reduce the complexity of the 3D scene input into our network. We represent the simplified 3D scene as a graph GN and input GN to our graph neural network Net_{GR} (Fig. 4) to encode the input 3D scene as an 8-dimensional latent vector. Then we pass the encoded 3D scene latent vector along with the listener position LP and the source position SP to our generator network Net_{GN} (Fig. 2) to generate binaural IR BIR (Equation 1).

$$BIR = Net_{GN}(Net_{GR}(GN), LP, SP). \quad (1)$$

3.1 Dataset Creation

There aren’t real-world and synthetic BIR datasets for a wide range of real 3D scenes captured using commodity hardware available to train our Scene2BIR. Therefore we create synthetic BIRs using a geometric simulator [Tang et al. 2020] for 3D reconstructed real-world scenes in the ScanNet dataset [Dai et al. 2017a] to train our Scene2BIR. We preprocess the 3D meshes and assign meaningful acoustic material properties to each object and surface in the 3D scene (§ 3.1.1). Next, we sample source and listener positions and simulate BIRs using the geometric simulator (§ 3.1.2).

3.1.1 Mesh Preprocessing and Material Assignment. The ScanNet dataset contains vertex-level segmented mesh with the semantic annotation (i.e., instance-level object category labels such as dish rack, wall, laundry basket etc.). In order to make the dataset compatible with a geometric propagation system, we convert vertex-level segmentation of the 3D scene to face-level segmentation of the 3D scene. Face-level segmentation is used to assign material acoustic coefficients to each surface in the 3D scene. Many of the meshes in the ScanNet dataset have holes on the surface boundary. The holes can prevent some of the sound rays from reflecting back to the listener and result in generating unrealistic sound effects using the ray tracing-based geometric propagation algorithm. We create the convex hull of the overall 3D scene mesh and merge it with the original mesh to close the holes. The ScanNet dataset contains the object labels for every 3D scene. We use the absorption coefficient acoustic database with more than 2,000 materials properties [Kling 2018] and assign the acoustic absorption coefficient for each individual surface or object materials in the 3D scenes using the acoustic material assignment approach proposed in GWA [Tang et al. 2022]. In addition to absorption coefficients, we need scattering coefficients for geometric sound propagation. The scattering coefficients are

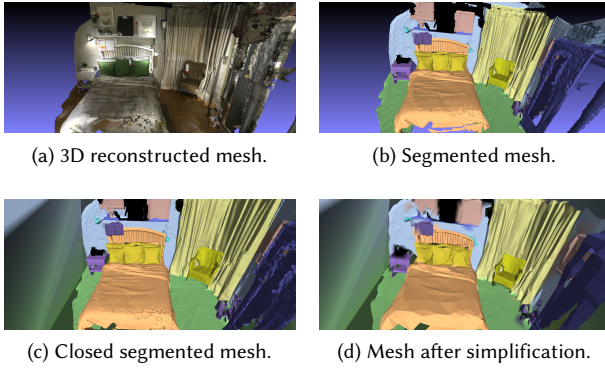


Fig. 3. The 3D reconstruction of the real scene from the ScanNet dataset (a), object category level segmentation of the 3D scene with each category is represented by a different color; (b) the modified mesh after closing the holes using convex hull; (c) the simplified mesh with object level segmentation information preserved; (d) we observe that high-level object shapes (e.g., bed, pillow, chair, table, etc.) and materials are preserved even after simplifying the mesh to 2.5% of the original size.

not available in the acoustic database [Kling 2018]. Therefore, we adapt the sampling approach proposed in GWA [2022]. We fit a Gaussian distribution by calculating the mean and standard deviation of 37 sets of scattering coefficients collected from the BRAS benchmark [Aspöck et al. 2020] and we sample randomly from the distribution for every 3D scene.

3.1.2 Geometric Sound Propagation. For every 3D scene, we perform grid sampling with 1m spacing in all three dimensions. We also ensure that there is a minimum gap of 0.2 m between sampled position and objects in the scene to prevent collisions. The number of grid samples varies with the dimension of the 3D scene. We randomly place 10 sources in the grid sampled locations and the rest of the samples are assigned to listener locations. We perform geometric simulations for every combination of listener and source positions. We use 20,000 rays for geometric propagation and the simulation stops when the maximum depth of specular or diffuse reflection is 2000 or the ray energy is below the hearing threshold.

4 OUR LEARNING APPROACH

In this section, we present the details of our learning method. Our approach learns to generate binaural impulse responses (BIRs) for 3D reconstructed real scenes, which may have noise or holes. We first present our approach of representing the topology and material details of the 3D scene using our graph neural network (§ 4.1). Next, we present our overall architecture, which takes the 3D scene and generates plausible BIRs and training details (§ 4.2).

4.1 3D Scene Representation

The ScanNet dataset represents the RGB-D data collected from the 3D scene in the form of a 3D mesh. The shape of the objects in the 3D scene is represented using the vertices and triangular faces in the 3D Cartesian coordinates. The ScanNet dataset also provides object category labels at the vertex level. We perform the mesh pre-processing and material assignment approach as mentioned in § 3.1.1. To reduce

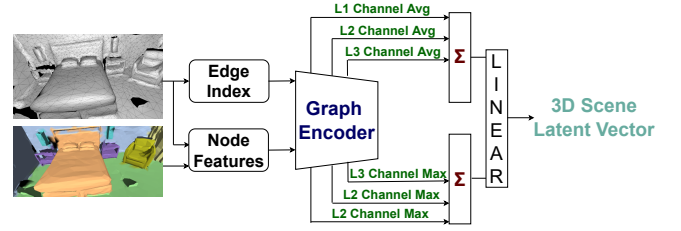


Fig. 4. Our network architecture represents a 3D scene as a 8-dimensional latent vector. The vertex positions and material properties are combined to produce the node features. We pass the edge index and node features from the 3D scene as input to the graph encoder. The graph encoder consists of 3 graph layers (L1, L2 and L3). The channel-wise average and the channel-wise maximum of the node features in each layer are aggregated and passed to linear layers. Linear layers output a 3D scene latent vector.

the size and complexity of the data passed to the neural network while preserving high-level object details, we perform mesh simplifications using PyMeshlab’s implementation of the quadratic-based edge collapse mesh simplification algorithm [Muntoni and Cignoni 2021]. We simplify the meshes to have only 2.5% of the initial number of faces. The mesh simplification algorithm can simplify the mesh while preserving the vertex-level segmentation of the mesh (Fig. 3). The simplified meshes typically have around 10,000 faces.

In Fig. 3, we observe that segmented mesh interpolates the nearby materials to the closed holes (e.g., holes near the floor are assigned to materials of the floor and the material is represented in green). We observe that even after mesh simplification to 2.5% of the original size, high-level object structures are preserved.

The triangular mesh of the 3D scene can be represented using graph $G = \langle V, E \rangle$, where V represents the 3D Cartesian coordinates of the set of vertices/nodes and E is the connectivity of each node (edge index). The vertex coordinates of three dimensions are features of the node in a graph. To add the material properties of the 3D scene, we increase the node feature dimension to five. The material properties can be represented using the material’s absorption coefficient and scattering coefficient. The absorption coefficient represents how much sound can be absorbed by the material. Metal absorbs the least sound and has a very low coefficient. A cushion is a sound-absorbing material and has a high coefficient. The scattering coefficient represents the roughness of the material’s surface. When the surface is rough, the sound will be scattered in all directions and has a high coefficient; smooth surfaces have a low coefficient value. The absorbing and scattering coefficients are frequency-dependent coefficients. The coefficients are defined for the 8-octave bands between 62.5 Hz and 8000 Hz. To reduce the dimensionality of the coefficients, we calculate the average coefficients by taking the coefficients at 500 Hz and 1000 Hz. In many practical applications, the average value of room acoustics parameters like reverberation time is used for analysis instead of all the values at different octave bands [Chen et al. 2022; Ratnarajah et al. 2021b; Tang et al. 2020]. We increase the node features V by combining (x, y, z) Cartesian coordinates of the vertex with the average absorption coefficient ab and average scattering coefficient sc ($V = [x, y, z, ab, sc]$).

We input node features and edge index to the graph encoder network to encode the 3D to low dimensional space. The encoder

network has 3 layers. In each layer, the graph convolution layer [Kipf and Welling 2017] is used to encode the node features (Equation 2). We gradually reduce the size of the graph by dropping the number of node features to 0.6 times the original number of node features in each layer using the graph pooling layer.

In Equation 2, the adjacency matrix representing the edge index of the 3D scene (A) and the identity matrix I are aggregated to calculate \hat{A} ($\hat{A} = A + I$). Each column of \hat{A} is summed to get diagonal matrix \hat{D} ($\hat{D}_{ii} = \sum_j \hat{A}_{ij}$). $W^{(n)}$ is a trainable weight matrix for layer n . Node features at layers n and $n + 1$ are $N_F^{(n)}$ and $N_F^{(n+1)}$, respectively.

$$N_F^{(n+1)} = \sigma(\hat{D}^{-\frac{1}{2}} \hat{A} \hat{D}^{-\frac{1}{2}} N_F^{(n)} W^{(n)}), \quad (2)$$

The output of the graph convolution layer is passed to the graph pooling layers [Gao and Ji 2019; Knyazev et al. 2019] to simplify the graph by reducing node features and edge index. The graph pooling layer initially calculates the square of the adjacency matrix ($A_{new}^{(n)} = A^{(n)} A^{(n)}$) to increase the graph connectivity and is used to choose top N node features. The adjacency matrix $A_{new}^{(n)}$ prevents isolated edges in the graph encoded 3D scene when choosing top N node features from the input graph and discarding other features.

We calculate the channel-wise average and channel-wise maximum of the output node features in each graph layer in the graph encoder network. We aggregate the channel-wise average and channel-wise maximum separately over the 3 layers. We concatenate the aggregated maximum and aggregated average values and pass them as input to a set of linear layers. We concatenate the learned features in each layer to ensure that the linear layers use all the learned features to construct an accurate 3D scene latent vector of dimension 8 as an output from the linear layer.

4.2 Binaural Impulse Response Generation

We use a one-dimensional modified conditional generative adversarial network (CGAN) to generate binaural impulse responses (BIR). The standard CGAN architectures [Gauthier 2015; Mirza and Osindero 2014] generate multiple different samples corresponding to input condition y by changing the input random noise vector z . In our CGAN architecture, we only input the condition y to generate a single precise output. Our CGAN network takes a 3D scene latent vector as the input condition and generates a single precise BIR. We propose a novel cost function to trigger the network to generate binaural effects such as interaural level difference (ILD) and interaural time difference (ITD) accurately.

We extend the IR preprocessing approach proposed in MESH2IR to make the network learn to generate BIRs with large variations of standard deviation (SD) efficiently. In § 3.1, we generate high-fidelity BIRs with a sampling rate of 48,000 Hz. We initially downsample the BIRs to 16,000 Hz to represent a longer duration of BIRs. We train our network to generate around 0.25 seconds (3968 samples) of BIR to reduce the complexity of the network. Our architecture can be easily modified to train the network to generate any duration of BIRs. The complexity of our network changes linearly with the duration of generated BIRs. We calculate the SD of the BIR and divide the BIR with SD to have fewer variations over training samples. We replicate the SD 128 times and concatenate it towards the end of the BIR. Therefore, each channel of the preprocessed BIR will

have 4096 samples (3968+128). We train our network to generate preprocessed BIR. Later we can recover the original BIR by removing SD represented in the last 128 samples, getting the average of SD values, and multiplying the first 3968 samples by the average SD value. We get the average SD over 128 samples to reduce the error of the recovered SD.

Our CGAN architecture consists of a generator network (G) and a discriminator network (D) (Fig. 2). We pass the 3D scene information Γ_S consisting of mesh topology and materials of the 3D scenes represented using a latent vector, and the listener and source position as an input to G . We train the G and the D in our CGAN architecture using our created BIRs (§ 3.1) and Γ_S in the data distribution p_{data} . We train G to minimize the objective function \mathcal{L}_G and the D to maximize the objective function \mathcal{L}_D alternately.

Generator objective function (\mathcal{L}_G): The \mathcal{L}_G is minimized during training to generate accurate BIRs for the given condition Γ_S . The \mathcal{L}_G (Equation 3) consists of modified CGAN error (\mathcal{L}_{CGAN}), BIR error (\mathcal{L}_{BIR}), ED error (\mathcal{L}_{ED}), and mean square error (\mathcal{L}_{MSE}). The contribution of each individual error is controlled using the weights λ_{BIR} , λ_{ED} and λ_{MSE} :

$$\mathcal{L}_G = \mathcal{L}_{CGAN} + \lambda_{BIR} \mathcal{L}_{BIR} + \lambda_{ED} \mathcal{L}_{ED} + \lambda_{MSE} \mathcal{L}_{MSE}. \quad (3)$$

The modified CGAN error is minimized when the BIRs generated using G are difficult to differentiate from the ground truth BIRs by D for each 3D scene Γ_S :

$$\mathcal{L}_{CGAN} = \mathbb{E}_{\Gamma_S \sim p_{data}} [\log(1 - D(G(\Gamma_S), \Gamma_S))]. \quad (4)$$

The time of arrival of the direct signal and the magnitude levels of the left and right channels of the BIRs significantly vary with the direction of the sound source. To make sure the network captures the relative variation of the IRs in left and right channels, we propose the BIR error formulation.

$$\mathcal{L}_{BIR} = \mathbb{E}_{(B_G, \Gamma_S) \sim p_{data}} [\mathbb{E}[(B_{LN}(\Gamma_S, s) - B_{RN}(\Gamma_S, s)) - (B_{LG}(\Gamma_S, s) - B_{RG}(\Gamma_S, s))^2]], \quad (5)$$

where B_{LN} and B_{RN} are the left and right channels of the BIRs generated using our network and B_{LG} and B_{RG} are the left and right channels of the ground truth BIRs.

The energy remaining in the BIR (b) with respect to the time t_i seconds and at frequency band with center frequency f_c Hz (Equation 6) is described using the energy decay relief (ED) [Jot 1992; Schroeder 1965]. The ED curves decay smoothly over time and they can be converted into an "equivalent impulse response" [Kuttruff 1993]. In previous works [Ratnarajah et al. 2022a,b], it is observed that ED helps the model to converge.

$$ED(b, t_i, f_c) = \sum_{t=i}^T |H(b, t, c)|^2. \quad (6)$$

The ED curves reduce exponentially over time. In previous works [Ratnarajah et al. 2022b], the mean square error (MSE) between ground truth BIR (B_G) and the generated BIR (B_N) is calculated. This approach does not capture the latter part of ED curves accurately. Therefore we compare the log of the ED curves between ground

truth and generated BIRs for each sample (s) as follows:

$$\mathcal{L}_{ED} = \mathbb{E}_{(B_G, \Gamma_S) \sim p_{data}} [\mathbb{E}_{c \sim C} [\mathbb{E}[(\log(ED(B_G(\Gamma_S), c, s)) - \log(ED(B_N(\Gamma_S), c, s)))^2]]]. \quad (7)$$

To capture the structures of the BIR, we also calculate MSE error in the time domain. For each 3D scene Γ_S we compare B_G and B_N over the samples (s) of BIR as follows:

$$\mathcal{L}_{MSE} = \mathbb{E}_{(B_G, \Gamma_S) \sim p_{data}} [\mathbb{E}[(B_G(\Gamma_S, s) - B_N(\Gamma_S, s))^2]]. \quad (8)$$

Discriminator objective function (\mathcal{L}_D): The discriminator (D) is trained to maximize the objective function \mathcal{L}_D (Equation 9) to differentiate the ground truth BIR (B_G) and the BIR generated using the generator (G) during training for each 3D scenes Γ_S .

$$\mathcal{L}_D = \mathbb{E}_{(B_G, \Gamma_S) \sim p_{data}} [\log(D(B_G(\Gamma_S), \Gamma_S))] + \mathbb{E}_{\Gamma_S \sim p_{data}} [\log(1 - D(G(\Gamma_S), \Gamma_S))]. \quad (9)$$

Network Architecture and Training: We extend the standard time domain Generator (G) and Discriminator (D) architectures proposed for monaural IR generation [Ratnarajah et al. 2022b,c]. We modify G to take our 3D scene latent vector of 8 dimensions (Fig. 4) and the source and listener positions in 3D Cartesian coordinates. Our G takes 14-dimensional conditional vectors and generates 4096x2 preprocessed BIR as output. We also modify our D to differentiate between 2 channel ground truth and generated BIRs. We train all networks with a batch size of 96 using RMSprop optimizer. We initially started with a learning rate of 8×10^{-5} and the learning rate decayed to 0.7 of its previous value every 7 epochs. We trained our network for 100 epochs.

5 ACOUSTIC EVALUATION

5.1 BRAS Benchmark

We use the BRAS benchmark [Aspöck et al. 2020] to evaluate the contribution of material properties to the accuracy of the BIR generated using our Scene2BIR method. The BRAS contains a complete scene description including the captured BIRs (i.e. ground truth) and the 3D models with semantic annotations for a wide range of scenes. We trained our approach without including the material properties (Scene2BIR-No-Material) and including material properties (Scene2BIR). We evaluate our approach using recorded BIRs from the chamber music hall and auditorium (Fig. 5). We generated BIRs corresponding to the source and listener positions in the same models and compared the accuracy. We plot the normalized early reflection energy decay curves (EDC) of the captured BIRs and the BIRs generated using our models (Fig. 5). The EDC describes the amount of energy remaining in the BIR with respect to time [Schroeder 1965]. We observe that in 2 different scenarios, adding material improves the energy decay pattern of the BIRs. We calculated the mean absolute error (MAE) between the EDC of captured BIRs and generated BIRs. MAE decreases by 3.6% for the medium room and 6.6% for the large room.

5.2 Accuracy Analysis

We quantitatively evaluate the accuracy of our proposed approach using standard acoustic metrics such as reverberation time (T_{60}),

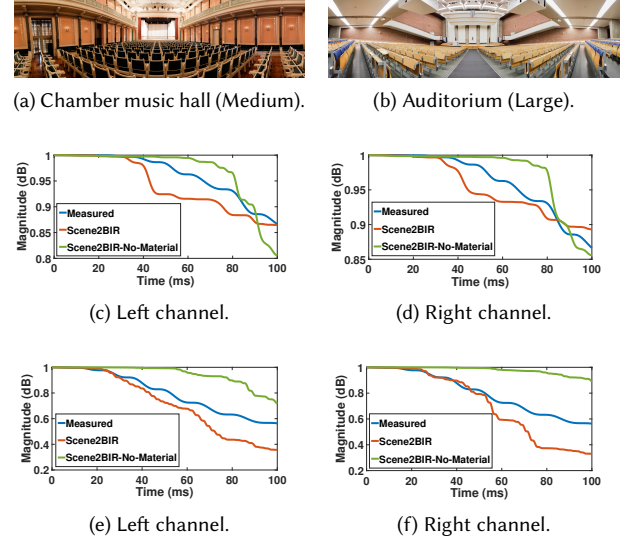


Fig. 5. The normalized energy decay curves (EDC) of the captured BIRs and the BIRs generated using our approach with material (Scene2BIR) and without material (Scene2BIR-No-Material) for the 3D scenes in BRAS ((a),(b)). We plot the EDC for the left and right channels of the BIRs from the chamber music hall ((c),(d)) and auditorium ((e),(f)). We observe that the EDC of Scene2BIR is closer to the EDC of captured BIRs.

direct-to-reverberant ratio (DRR), and early-decay-time (EDT). T_{60} measures the time taken for the sound pressure to decay by 60 decibels (dB). The ratio of the sound pressure level of the direct sound to the sound arriving after surface reflections is DRR [Naylor and Gaubitch 2010]. The six times the time taken for the sound pressure to decay by 10 dB corresponds to EDT. We generate 2000 high-quality BIRs using a large number of rays with geometric sound propagation [Schissler and Manocha 2017] for 166 real-world scenes not used to train our networks in the ScanNet dataset. We compare the accuracy of Scene2IR with the IRs computed using geometric sound propagation on these scenes.

We calculate the mean absolute acoustic metrics error of the BIRs generated using our approach with materials (Scene2BIR) and without materials (Scene2BIR-No-Material). We report the average error from 2 channels in our generated BIRs (Table 1). Many prior learning-based approaches are not capable of generating IRs for new scenes not used during training [Luo et al. 2022] or generating BIRs for standard inputs taken by physics-based BIR simulators [Majumder et al. 2022]. MESH2IR [2022b] can generate monaural IRs from 3D mesh models. Therefore, we compare the acoustic metrics of MESH2IR separately with the left and right channels and report the average error. We highlight the accuracy improvements in Table 1.

6 PERCEPTUAL EVALUATION

We perceptually evaluate the sounds rendered using Scene2BIR and compare them with prior learning-based and geometric sound propagation algorithms. The purpose of our study is to verify whether the sound rendered using our Scene2BIR is plausible (with left and right

Table 1. We calculate the mean absolute reverberation time (T_{60}) error, direct-to-reverberant ratio (DRR) error and early-decay-time (EDT) error for IRs generated using MESH2IR and BIRs generated using our approach with materials (Scene2BIR) and without material (Scene2BIR-No-Material). We compare them with BIRs computed using geometric sound propagation methods (§ 3.1). We compare the monaural IRs generated using MESH2IR with each channel in BIRs separately and compute the average. We observe 48% accuracy improvement of EDC error with our Scene2BIR when compared to MESH2IR. The best results of each metric are shown in **bold**.

IR Dataset	Mean Absolute Error ↓		
	T_{60} (s)	DRR (dB)	EDT (s)
MESH2IR [Ratnarajah et al. 2022b]	0.16	5.06	0.25
Scene2BIR-No-Material	0.10	3.15	0.14
Scene2BIR	0.08	1.7	0.13

Table 2. The participants’ responses on how plausible the sounds in each video were created using 3D scenes in the ScanNet dataset. We compare auralized video using our Scene2BIR approach with the auralized videos using clean speech, MESH2IR, and Scene2BIR-No-Material. We compare Scene2BIR-No-Material using a single source in medium (M) and large (L) 3D scenes. We observe that 67% of the participants prefer Scene2BIR when we play video generated using Scene2BIR and MESH2IR with a single source. The highest comparative percentage is **bolded**.

Baseline Method	No of Sources	Baseline	No Preference	Scene2BIR
Clean	1	27.14%	1.43%	71.43%
	2	17.14%	2.86%	80%
Mesh2IR [Ratnarajah et al. 2022b]	1	30%	2.86%	67.14%
	2	15.71%	5.71%	78.57%
Scene2BIR-No-Material	1 (M)	30%	20%	50%
	1 (L)	22.85%	11.43%	65.71%
	2	22.86%	17.14%	60%

channels). We auralized three scenes with a single sound source and 2 scenes with two sound sources from the ScanNet test dataset (more details in the video). We created a 40-second video of each scene by moving the listener around the scene. We evaluate our approach by adding sounds generated using different methods to the 3D scene walkthrough: clean or dry sound (Clean), sound propagation effects created using MESH2IR, Scene2BIR-No-Material and Scene2BIR. We also compared the reverberant speech created using Scene2BIR-No-Material and Scene2BIR with the captured IRs from two different scenes in the BRAS dataset (Fig. 5). We conducted our user study using Amazon Mechanical Turk (AMT) with 70 participants (47 males and 23 females). The average completion time of our user study is 20 minutes for each user. We performed the following comparisons in perceptual evaluation:

Clean vs. Scene2BIR: We compared sound-rendered 3D scenes with a single sound source and 2 sound sources. In this experiment, we evaluate whether our approach creates continuous and smooth sound effects when moving around the scene and whether the user can perceive the indirect sound effects.

MESH2IR vs. Scene2BIR: We generated auralized video each for a single source and 2 sources. Our goal is to investigate whether the participants feel that the sound effects in the left and right ears change smoothly and synchronously as the user walks in the scene.

In addition to distance, we investigate whether our sound effects change smoothly with the direction of the source.

Scene2BIR-No-Material vs. Scene2BIR: We auralized two scenes with a single source from a medium-sized and a large scene, and another scene with two sources. In this experiment, we evaluate whether the reverberation effects from Scene2BIR match closely with the environment when compared with Scene2BIR-No-Material. Our goal is to evaluate the perceptual benefits of adding material characteristics in our learning method.

In our experiment, we randomly choose the location of two videos (left or right) used for the comparison and ask the participants to rate from -2 to +2 based on which video sounds more plausible, i.e. the way the sound varies in both ears when the listener moves towards and away from the sound source. The participants rate -2 if the left video sounds more plausible and vice versa. If the participants have no preference, they rate 0. We group the negative scores (-1 and -2) and positive scores (1 and 2) to choose the participants’ preferences.

We summarize the participants’ responses in Table 2. We observe that 67% - 79% of the participants observe that the auralized scenes with 1-2 sources using Scene2BIR are more plausible than MESH2IR. We also observe that when there is more than one source in the 3D scene, the relative sound variation of the sources based on their location is more plausible with Scene2BIR, as compared to using dry sound or MESH2IR. In large 3D models, where the T_{60} tends to be higher, 66% of participants feel Scene2BIR is more plausible than Scene2BIR-No-Material.

We also played reverberant speech created using captured left channel IRs from the BRAS and left channel IRs generated using our Scene2BIR and Scene2BIR-No-Material in two different 3D scenes (Fig. 5). We use single-channel IRs to remove sound effects from ITD and ILD and make the participants focus on reverberation effects. We asked the participants to choose which speech sampled auralized using our BIRs is closer to the real speech from the BRAS. In the medium-sized music hall 55.7% selected Scene2BIR. In the large auditorium, 78.6% of the participants observe reverberant speech from Scene2BIR is closer to real speech. Our user study results highlight the benefits of Scene2IR over prior methods.

7 CONCLUSION, LIMITATIONS AND FUTURE WORK

We present a material-aware binaural impulse response (BIR) generator to generate thousands of BIRs on the fly for a given real-world 3D scene. We propose a novel approach to handle material properties in our network. Moreover, we show that adding material information significantly improves the accuracy of BIR generation and is comparable to geometric propagation methods or captured BIRs in terms of acoustic characteristics and perceptual evaluation. Overall, our algorithm offers two orders of magnitude performance improvement over interactive geometric sound propagation methods.

Our approach has some limitations. The performance of our network depends on the training data. We can train our network with real-world captured BIRs, though it is challenging and expensive to capture a large number of such BIRs. Currently, we use BIRs generated using sound propagation algorithms for training, and the overall accuracy of Scene2IR is also a function of the accuracy of the training data. Our approach is limited to static real-world

scenes. Our material classification methods assume that accurate semantic labels for each object in the scene are known. It is possible to consider sub-band acoustic material coefficients to further improve the accuracy. However, the complexity of the graph representation of the 3D scene drastically increases and we are limited by the GPU memory to handle such complex graphs. As part of our future work, we would like to evaluate the performance on other real-world reconstructed models.

REFERENCES

- Andrew Allen and Nikunj Raghuvanshi. 2015. Aerophones in flatland: interactive wave simulation of wind instruments. *ACM Trans. Graph.* 34, 4 (2015), 134:1–134:11.
- Lukas Aspöck, Michael Vorländer, Fabian Brinkmann, David Ackermann, and Stefan Weinzierl. 2020. Benchmark for Room Acoustical Simulation (BRAS). *DOI* 10 (2020), 14279.
- Fabian Brinkmann, Lukas Aspöck, David Ackermann, Steffen Lepa, Michael Vorländer, and Stefan Weinzierl. 2019. A round robin on room acoustical simulation and auralization. *The Journal of the Acoustical Society of America* 145, 4 (2019), 2746–2760.
- Changan Chen, Carl Schissler, Sanchit Garg, Philip Kobernik, Alexander Clegg, Paul Calamia, Dhruv Batra, Philip W Robinson, and Kristen Grauman. 2022. Soundspaces 2.0: A simulation platform for visual-acoustic learning. *arXiv preprint arXiv:2206.08312* (2022).
- Angela Dai, Angel X. Chang, Manolis Savva, Maciej Halber, Thomas A. Funkhouser, and Matthias Nießner. 2017a. ScanNet: Richly-Annotated 3D Reconstructions of Indoor Scenes. In *CVPR*. IEEE Computer Society, 2432–2443.
- Angela Dai, Matthias Nießner, Michael Zollhöfer, Shahram Izadi, and Christian Theobalt. 2017b. BundleFusion: Real-Time Globally Consistent 3D Reconstruction Using On-the-Fly Surface Reintegration. *ACM Trans. Graph.* 36, 4, Article 76a (jul 2017), 18 pages. <https://doi.org/10.1145/3072959.3054739>
- James Eaton, Nikolay D. Gaubitch, Alastair H. Moore, and Patrick A. Naylor. 2016. Estimation of Room Acoustic Parameters: The ACE Challenge. *IEEE/ACM Transactions on Audio, Speech, and Language Processing* 24, 10 (2016), 1681–1693. <https://doi.org/10.1109/TASLP.2016.2577502>
- Hongyang Gao and Shuiwang Ji. 2019. Graph U-Nets. In *ICML (Proceedings of Machine Learning Research, Vol. 97)*. PMLR, 2083–2092.
- Jon Gauthier. 2015. Conditional generative adversarial networks for convolutional face generation. In *Tech Report*.
- Andrea F. Genovesi, Hannes Gamper, Ville Pulkki, Nikunj Raghuvanshi, and Ivan J. Tashev. 2019. Blind Room Volume Estimation from Single-channel Noisy Speech. In *ICASSP 2019 - 2019 IEEE International Conference on Acoustics, Speech and Signal Processing (ICASSP)*. 231–235. <https://doi.org/10.1109/ICASSP.2019.8682951>
- Nail A. Gumerov and Ramani Duraiswami. 2008. A Broadband Fast Multipole Accelerated Boundary Element Method for the 3D Helmholtz Equation.
- Jean-Marc Jot. 1992. An analysis/synthesis approach to real-time artificial reverberation. In *ICASSP*. IEEE Computer Society, 221–224.
- Thomas N. Kipf and Max Welling. 2017. Semi-Supervised Classification with Graph Convolutional Networks. In *ICLR (Poster)*. OpenReview.net.
- Christoph Kling. 2018. Absorption coefficient database. <https://www.ptb.de/cms/de/ptb/fachabteilungen/abt1/fb-16/ag-163/absorption-coefficient-database.html>
- Boris Knyazev, Graham W. Taylor, and Mohamed R. Amer. 2019. Understanding Attention and Generalization in Graph Neural Networks. In *NeurIPS*. 4204–4214.
- Homare Kon and Hideki Koike. 2019. Estimation of late reverberation characteristics from a single two-dimensional environmental image using convolutional neural networks. *Journal of the audio engineering society* 67, 7/8 (July 2019), 540–548. <https://doi.org/10.17743/jaes.2018.0069>
- Heinrich Kuttruff. 1993. Auralization of impulse responses modeled on the basis of ray-tracing results. *Journal of the audio engineering society* 41, 11 (November 1993), 876–880.
- Heinrich Kuttruff. 2016. *Room acoustics*. Crc Press.
- Pontus Larsson, Daniel Västfjäll, and Mendel Kleiner. 2002. Better presence and performance in virtual environments by improved binaural sound rendering. In *Audio Engineering Society Conference: 22nd International Conference: Virtual, Synthetic, and Entertainment Audio*. Audio Engineering Society.
- Tobias Lentz, Dirk Schröder, Michael Vorländer, and Ingo Assenmacher. 2007. Virtual Reality System with Integrated Sound Field Simulation and Reproduction. *EURASIP J. Adv. Signal Process* 2007, 1 (jan 2007), 187. <https://doi.org/10.1155/2007/70540>
- Dingzeyu Li, Timothy R. Langlois, and Changxi Zheng. 2018. Scene-Aware Audio for 360° Videos. *ACM Trans. Graph.* 37, 4, Article 111 (jul 2018), 12 pages. <https://doi.org/10.1145/3197517.3201391>
- Chenxi Liu, Alexander G. Schwing, Kaustav Kundu, Raquel Urtasun, and Sanja Fidler. 2015. Rent3D: Floor-plan priors for monocular layout estimation. In *CVPR*. IEEE Computer Society, 3413–3421.
- Qi Liu, Matt J Kusner, and Phil Blunsom. 2020. A survey on contextual embeddings. *arXiv preprint arXiv:2003.07278* (2020).
- Shiguang Liu and Dinesh Manocha. 2022. Sound Synthesis, Propagation, and Rendering. *Synthesis Lectures on Visual Computing: Computer Graphics, Animation, Computational Photography, and Imaging* 11, 2 (2022), 1–110.
- Andrew Luo, Yilun Du, Michael J Tarr, Joshua B Tenenbaum, Antonio Torralba, and Chuang Gan. 2022. Learning Neural Acoustic Fields. *arXiv preprint arXiv:2204.00628* (2022).
- Sagnik Majumder, Changan Chen, Ziad Al-Halah, and Kristen Grauman. 2022. Few-Shot Audio-Visual Learning of Environment Acoustics. *arXiv preprint arXiv:2206.04006* (2022).
- Ravish Mehra, Nikunj Raghuvanshi, Lakulish Antani, Anish Chandak, Sean Curtis, and Dinesh Manocha. 2013. Wave-based sound propagation in large open scenes using an equivalent source formulation. *ACM Trans. Graph.* 32, 2 (2013), 19:1–19:13.
- Ravish Mehra, Atul Rungta, Abhinav Golas, Ming Lin, and Dinesh Manocha. 2015. WAVE: Interactive Wave-based Sound Propagation for Virtual Environments. *IEEE Transactions on Visualization and Computer Graphics* 21, 4 (2015), 434–442. <https://doi.org/10.1109/TVCG.2015.2391858>
- Mehdi Mirza and Simon Osindero. 2014. Conditional Generative Adversarial Nets. *arXiv preprint arXiv:1411.1784* (2014).
- Mridul K Mishra and Jaydeep Viradiya. 2019. Survey of Sentence Embedding Methods. *International Journal of Applied Science and Computations* 6, 3 (2019), 592–592.
- Alessandro Muntoni and Paolo Cignoni. 2021. PyMeshLab. <https://doi.org/10.5281/zenodo.4438750>
- P A Naylor and N D Gaubitch. 2010. *Speech Dereverberation* (1st ed.). Springer Publishing Company, Incorporated.
- Nikunj Raghuvanshi, Rahul Narain, and Ming C. Lin. 2009. Efficient and Accurate Sound Propagation Using Adaptive Rectangular Decomposition. *IEEE Trans. Vis. Comput. Graph.* 15, 5 (2009), 789–801.
- Nikunj Raghuvanshi, John M. Snyder, Ravish Mehra, Ming C. Lin, and Naga K. Govindaraju. 2010. Precomputed wave simulation for real-time sound propagation of dynamic sources in complex scenes. *ACM Trans. Graph.* 29, 4 (2010), 68:1–68:11.
- Anton Ratnarajah, Ishwarya Ananthabhotla, Vamsi Krishna Ithapu, Pablo Hoffmann, Dinesh Manocha, and Paul Calamia. 2022a. Towards Improved Room Impulse Response Estimation for Speech Recognition. *arXiv preprint arXiv:2211.04473* (2022).
- Anton Ratnarajah, Zhenyu Tang, Rohith Aralikatti, and Dinesh Manocha. 2022b. MESH2IR: Neural Acoustic Impulse Response Generator for Complex 3D Scenes. In *ACM Multimedia*. ACM, 924–933.
- Anton Ratnarajah, Zhenyu Tang, and Dinesh Manocha. 2021a. IR-GAN: Room Impulse Response Generator for Far-Field Speech Recognition. In *Interspeech*. ISCA, 286–290.
- Anton Ratnarajah, Zhenyu Tang, and Dinesh Manocha. 2021b. TS-RIR: Translated Synthetic Room Impulse Responses for Speech Augmentation. In *2021 IEEE Automatic Speech Recognition and Understanding Workshop (ASRU)*. 259–266. <https://doi.org/10.1109/ASRU51503.2021.9688304>
- Anton Ratnarajah, Shi-Xiong Zhang, Meng Yu, Zhenyu Tang, Dinesh Manocha, and Dong Yu. 2022c. Fast-Rir: Fast Neural Diffuse Room Impulse Response Generator. In *ICASSP*. IEEE, 571–575.
- Zhimin Ren, Hengchin Yeh, and Ming C Lin. 2013. Example-guided physically based modal sound synthesis. *ACM Transactions on Graphics (TOG)* 32, 1 (2013), 1–16.
- Lauri Savioja. 2010. Real-time 3D finite-difference time-domain simulation of low-and mid-frequency room acoustics. In *13th Int. Conf on Digital Audio Effects*, Vol. 1. 75.
- Lauri Savioja and U. Peter Svensson. 2015. Overview of geometrical room acoustic modeling techniques. *The Journal of the Acoustical Society of America* 138, 2 (2015), 708–730. <https://doi.org/10.1121/1.4926438> arXiv:<https://doi.org/10.1121/1.4926438>
- Carl Schissler, Christian Loftin, and Dinesh Manocha. 2017. Acoustic classification and optimization for multi-modal rendering of real-world scenes. *IEEE transactions on visualization and computer graphics* 24, 3 (2017), 1246–1259.
- Carl Schissler and Dinesh Manocha. 2011. gsound: interactive sound propagation for games. *journal of the audio engineering society* (february 2011).
- Carl Schissler and Dinesh Manocha. 2017. Interactive Sound Propagation and Rendering for Large Multi-Source Scenes. *ACM Trans. Graph.* 36, 1 (2017), 2:1–2:12.
- Carl Schissler, Ravish Mehra, and Dinesh Manocha. 2014. High-Order Diffraction and Diffuse Reflections for Interactive Sound Propagation in Large Environments. *ACM Trans. Graph.* 33, 4, Article 39 (jul 2014), 12 pages. <https://doi.org/10.1145/2601097.2601216>
- M. R. Schroeder. 1965. New Method of Measuring Reverberation Time. *The Journal of the Acoustical Society of America* 37, 6 (1965), 1187–1188. <https://doi.org/10.1121/1.1939454> arXiv:<https://doi.org/10.1121/1.1939454>
- Hoda S Seddeq. 2009. Factors influencing acoustic performance of sound absorptive materials. *Australian journal of basic and applied sciences* 3, 4 (2009), 4610–4617.
- Nikhil Singh, Jeff Mentch, Jerry Ng, Matthew Beveridge, and Iddo Drori. 2021. Image2Reverb: Cross-Modal Reverb Impulse Response Synthesis. In *ICCV*. IEEE, 286–295.
- Christian J. Steinmetz, Vamsi Krishna Ithapu, and Paul Calamia. 2021. Filtered Noise Shaping for Time Domain Room Impulse Response Estimation from Reverberant Speech. In *2021 IEEE Workshop on Applications of Signal Processing to Audio and*

- Acoustics (WASPAA). 221–225. <https://doi.org/10.1109/WASPAA52581.2021.9632680>
- Kun Su, Mingfei Chen, and Eli Shlizerman. 2022. INRAS: Implicit Neural Representation for Audio Scenes. In *Advances in Neural Information Processing Systems*, Alice H. Oh, Alekh Agarwal, Danielle Belgrave, and Kyunghyun Cho (Eds.). <https://openreview.net/forum?id=7KBzV5IL7W>
- Zhenyu Tang, Rohith Aralikatti, Anton Jeran Ratnarajah, and Dinesh Manocha. 2022. GWA: A Large High-Quality Acoustic Dataset for Audio Processing. In *SIGGRAPH (Conference Paper Track)*. ACM, 36:1–36:9.
- Zhenyu Tang, Nicholas J Bryan, Dingzeyu Li, Timothy R Langlois, and Dinesh Manocha. 2020. Scene-aware audio rendering via deep acoustic analysis. *IEEE transactions on visualization and computer graphics* 26, 5 (2020), 1991–2001.
- Z. Tang, L. Chen, B. Wu, D. Yu, and D. Manocha. 2020. Improving Reverberant Speech Training Using Diffuse Acoustic Simulation. In *ICASSP 2020 - 2020 IEEE International Conference on Acoustics, Speech and Signal Processing (ICASSP)*. 6969–6973.
- Zhenyu Tang, Hsien-Yu Meng, and Dinesh Manocha. 2021. Learning Acoustic Scattering Fields for Dynamic Interactive Sound Propagation. In *2021 IEEE Virtual Reality and 3D User Interfaces (VR)*. 835–844. <https://doi.org/10.1109/VR50410.2021.00111>
- Lonny L. Thompson. 2006. A review of finite-element methods for time-harmonic acoustics. *The Journal of the Acoustical Society of America* 119, 3 (2006), 1315–1330. <https://doi.org/10.1121/1.2164987> arXiv:<https://doi.org/10.1121/1.2164987>
- Frederic L. Wightman and Doris J. Kistler. 1992. The dominant role of low-frequency interaural time differences in sound localization. *The Journal of the Acoustical Society of America* 91 3 (1992), 1648–61.

A SUPPLEMENTARY MATERIAL

A.1 Supplementary Video

Our supplementary video shows the full pipeline of adding sound effects to the real-world environment. We initially show how ScanNet 3D reconstruction is generated from video captured using iPad and Microsoft Kinect. Then we show how we can auralize the reconstructed 3D scene using our pipeline.

We also compare the auralized scenes using our Scene2BIR with auralized scenes using clean speech, MESH2IR [Ratnarajah et al. 2022b], Scene2BIR-No-Material and a geometric-based approach [Schissler and Manocha 2017]. At last, we compare the reverberant speech created using recorded IRs from the BRAS dataset [Aspöck et al. 2020] in 2 different environments (Chamber music hall and Auditorium) with reverberant speech created using our Scene2BIR for the same listener and source positions in the 2 different environments.

A.2 Time-domain comparison of BIRs [Geometric-based vs Scene2BIR(Ours)]

We plot additional time-domain representation of binaural impulse responses (BIR) generated using a geometric-based approach [Schissler and Manocha 2017] and our proposed Scene2BIR (Fig. 6, Fig. 7 and Fig. 8). We can see that the amount of reverberation and the high-level structures of the BIRs generated using our approach matches BIRs generated using the geometric-based method. Also, we can see that the interaural level difference and interaural time difference in our generated BIRs match the BIRs from a geometric-based method.

A.3 Acoustic absorption coefficient assignment to ScanNet 3D Scenes

The ScanNet dataset contains the object labels (e.g., dish rack, wall, laundry basket etc.) for every 3D scene. We use the absorption coefficient acoustic database with more than 2000 materials [Kling 2018] to get the absorption coefficient of each material in the ScanNet 3D reconstructions. We do not always find exact ScanNet object labels in the acoustic database. Therefore, we use the natural language processing (NLP) technique to find the closest matching material in the acoustic database for every ScanNet object label and assign

its absorption coefficient to the ScanNet object label. To find the closest matching material, we encode the object labels in ScanNet and material names in the acoustic database into fixed-length sentence embeddings [Mishra and Viradiya 2019]. Transformer-based sentence embedding vectors are close in cosine similarity distance for sentences with similar meaning and outperform in many NLP tasks [Liu et al. 2020]. We use the Microsoft pre-trained sentence transformer model to encode materials into 768-dimensional sentence embedding. We use the cosine similarity of the ScanNet object labels and materials in the acoustic database and assign the closest materials absorption coefficients to the objects in the ScanNet.

A.4 Code for generating BIRs using Scene2BIR

We have provided the code to generate BIRs using our trained Scene2BIR model. Our code will generate BIRs for 2 different sources in the 3D scene. We generated 1000 BIRs for each source with different listener locations in the 3D scene. Go inside **Scene2BIR** folder and run the command **source run.sh** to generate BIRs. The generated BIRs can be found inside the folder **Output/scene0000_02**. There are 2 separate folders "S1" and "S2" for each sound source.

A.5 Run time

We generated 2500 BIRs for a given 3D scene to calculate the run time. Our network consists of a graph neural network (GNN) and a BIR generator network. For a given 3D scene, we perform mesh encoding using GNN only once and we generate BIRs by varying source and listener positions. On average, our network takes 0.21 seconds to encode the scene using GNN and 0.023 milliseconds to generate a BIR. Therefore on average, our network takes 0.1 milliseconds to generate 2500 BIRs for a given 3D scene.

Fig. 6. The binaural impulse response (BIR) generated for real-world 3D reconstructed scenes captured using commodity hardware. The BIRs are generated offline using a geometric acoustic simulator (Top) and on-the-fly using our Scene2BIR network (Bottom) for new 3D scenes not used for training.

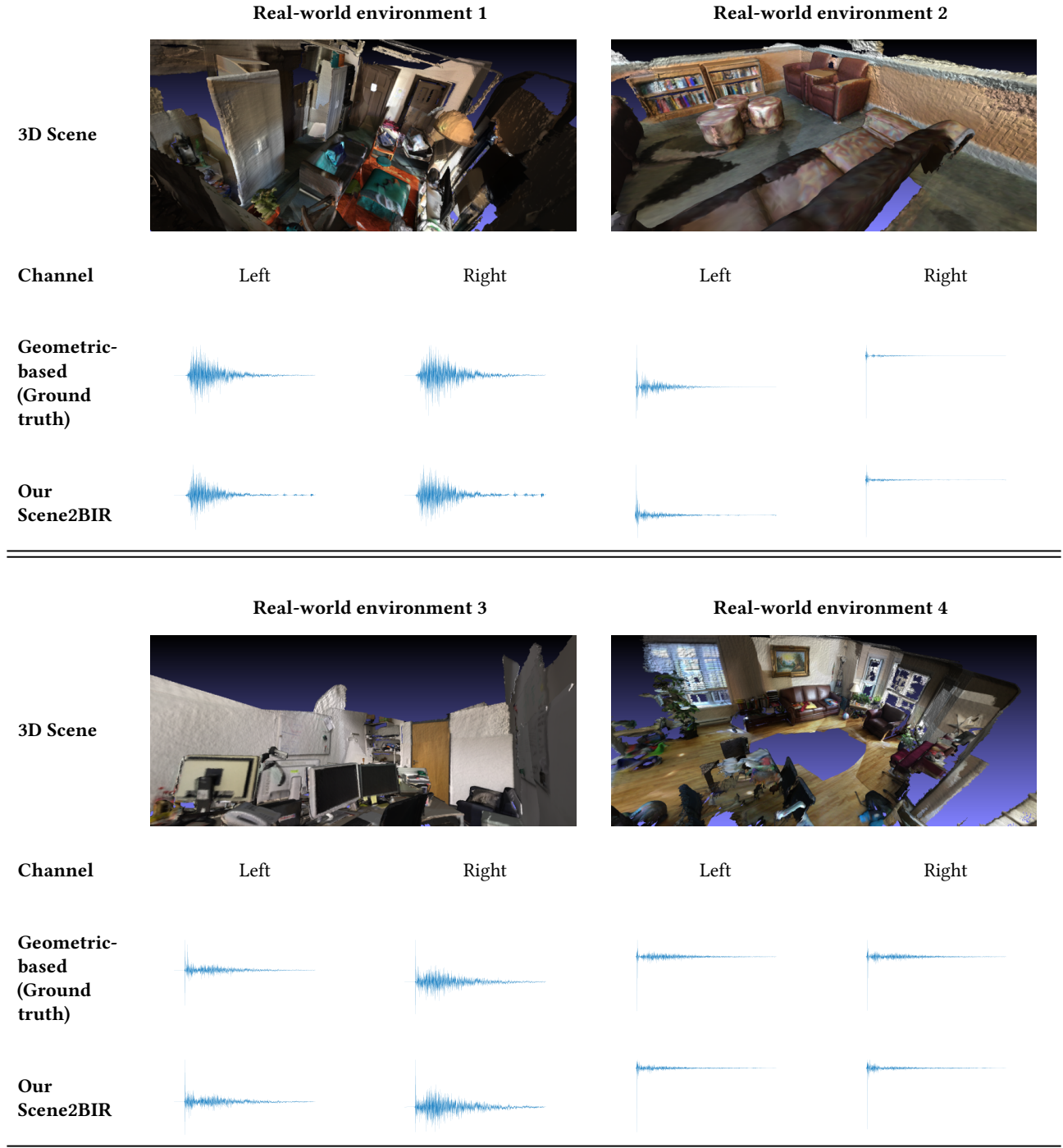


Fig. 7. The binaural impulse response (BIR) generated for real-world 3D reconstructed scenes captured using commodity hardware. The BIRs are generated offline using a geometric acoustic simulator (Top) and on-the-fly using our Scene2BIR network (Bottom) for new 3D scenes not used for training.

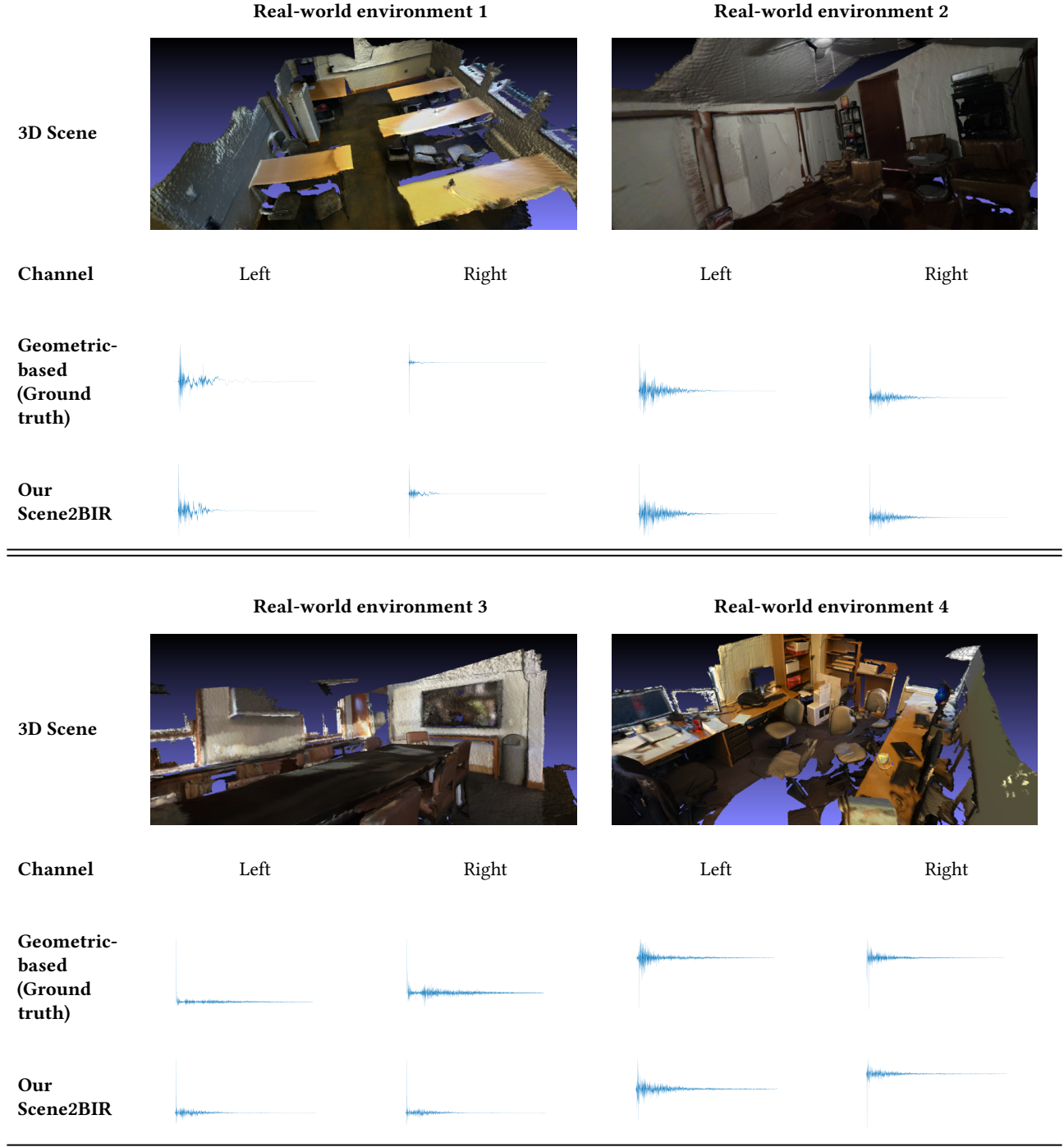


Fig. 8. The binaural impulse response (BIR) generated for real-world 3D reconstructed scenes captured using commodity hardware. The BIRs are generated offline using a geometric acoustic simulator (Top) and on-the-fly using our Scene2BIR network (Bottom) for new 3D scenes not used for training.

